Reconfigurable magnetic domain wall pinning using vortex-generated magnetic fields

Aaron Hurst, Joshua A. Izaac, Fouzia Altaf, Vincent Baltz, Peter J. Metaxas

Reconfigurable magnetic domain wall pinning using vortex-generated magnetic fields

Aaron C. H. Hurst,[1] Joshua A. Izaac,[1] Fouzia Altaf,[1] Vincent Baltz,[2] and Peter J. Metaxas[1,a)]
[1]*School of Physics and Astrophysics, M013, University of Western Australia, 35 Stirling Hwy, Crawley, WA 6009, Australia*
[2]*SPINTEC, Univ. Grenoble Alpes/CNRS/INAC-CEA, F-38000 Grenoble, France*

(Received 8 February 2017; accepted 13 April 2017; published online 2 May 2017)

Although often important for domain wall device applications, reproducible fabrication of pinning sites at the nano-scale remains challenging. Here, we demonstrate that the stray magnetic field generated beneath magnetic vortex cores can be used to generate localized pinning sites for magnetic domain walls in an underlying, perpendicularly magnetized nanostrip. Moreover, we show that the pinning strength can be tuned by switching the vortex core polarity: switching the core polarity so that it is aligned with the magnetization of the expanding domain (rather than against it) can reduce the vortex-mediated wall depinning field by between 40% and 90%, depending on the system geometry. Significant reductions in the depinning field are also demonstrated in narrow strips by shifting the core away from the strips' centers. *Published by AIP Publishing.*
[http://dx.doi.org/10.1063/1.4982237]

Control of magnetic domain wall (DW) motion is critical for the realization of DW devices such as logic circuits and (multi-state) memories.[1–6] Such devices are typically based upon ferromagnetic strips through which DWs propagate. In strips, stable positions for DWs have traditionally been achieved by structural modifications, often via the creation of local constrictions or protrusions[7] (local modifications to anisotropy have also been employed, e.g., Ref. 8). However, uniform fabrication of structural pinning sites at the nano-scale can be challenging. Another challenge is the need to balance the positional stability afforded by strong pinning sites (critical for data endurance) with a technological requirement for low power domain wall motion/depinning.[9]

A potential solution to the latter challenge is to use pinning sites whose strength can be dynamically modified, enabling, for example, the pinning strength to be (momentarily) reduced when the domain wall position has to be changed. Voltage-induced domain wall gating is one potential route to realize such pinning.[11,12] However, reconfigurable pinning can also be generated using stray magnetic fields from neighboring ferromagnetic elements.[13–18] Using ferromagnetic elements in this way also enables *nonvolatile* reconfigurability since the magnetic state of the element can be switched, modifying the stray field profile and thus the strength of the resulting pinning site.

Previous studies of stray-field-mediated pinning have focused primarily on the use of (quasi-)uniformly magnetized, bistable ferromagnetic elements.[4,13,15,18] In this letter, we use micromagnetic simulation to demonstrate the potential of magnetic vortices[19–21] for DW pinning (see also Ref. 22). Like DWs,[23] magnetic vortices are inherently reconfigurable and non-uniform magnetization configurations. They can exist within ferromagnetic disks and consist of an in-plane curling magnetization with an out of plane magnetized nano-scale core. Here, we use the highly localized stray magnetic field which exists around the core (and which is parallel to the core magnetization[20,21,24]) to pin domain walls in an underlying strip. We show that by switching the core magnetization (which is perpendicular to the disk plane and can be (rapidly) switched[25–29]), it is possible to toggle between strong and weak DW pinning sites. However, we also show that the pinning strength can also be varied by shifting the core away from the center of the strip, adding an additional degree of tunability without requiring a reversal of the core magnetization. Finally, we note that this approach to pinning enables one to create a pinning site with a reliable characteristic width and strength without the need to accurately and reproducibly fabricate similar nano-scaled structural features. This is because the core size is largely independent of the disk width (for those disks which exhibit a single vortex state: ≈100 nm up to the micrometer scale).[30]

Vortex-mediated DW pinning was studied in a 3 nm thick strip with perpendicular magnetic anisotropy. Two vortex-containing disks with a diameter of 192 nm and a thickness of 12 nm lie above the strip [Fig. 1(a)]. There is a vertical separation, d, between the bottom of the disks and the top of the strip [Fig. 1(b)]. The 768 nm long strip is CoPtCr-like[31] with saturation magnetization $M_S = 300$ kA/m, out-of-plane uniaxial anisotropy $K = 0.2$ MJ/m^3, and exchange stiffness $A_{ex} = 10$ pJ/m. The disks are NiFe-like with $M_S = 860$ kA/m, $A_{ex} = 13$ pJ/m, and negligible intrinsic anisotropy. The damping parameter

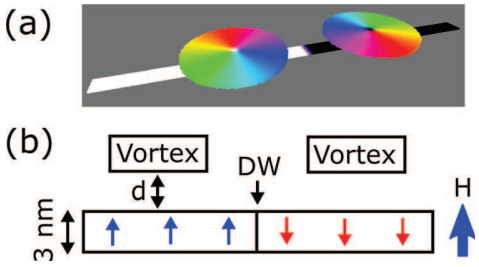

FIG. 1. System schematics. (a) 2 vortices above a DW-containing strip in the zero external field (visualized using Muview2[10]). (b) Side view schematic (not to scale) showing the finite separation, d, between the lower surface of the disks and the upper surface of the strip.

a)Electronic mail: peter.metaxas@uwa.edu.au

is 1 everywhere since we consider relaxed states only. No temperature effects were included nor was inter-element exchange coupling, meaning that the disk-layer interaction is purely magnetostatic. The disks are symmetrically spaced either side of the center of the strip along the strip's long axis. The majority of the presented data has been obtained with MuMax3[32] using $3 \times 3 \times 3\,\mathrm{nm}^3$ discretization cells. Good consistency with OOMMF[33] results was also found, which is mentioned below. For both approaches, the system was initialized with a DW-like transition at the middle of the strip and trial vortex configurations in the disks (the vortex chiralities are anti-clockwise unless otherwise specified). The magnetization was then allowed to relax in the zero external field using MuMax3's "minimize" routine (or OOMMF's "relax" routine). Both routines employ a conjugate gradient method to find the ground state magnetization. From this point, the simulation was progressed in a quasi-static manner. An external magnetic field, $H_{ext} = (0, 0, H)$ [Fig. 1(b)], was applied and increased in steps of ΔH starting at the zero field. The minimize/relax routine was run at each field value, starting from the relaxed configuration obtained at the previous field. The system's relaxed configuration was recorded after each step. Note that H was always positive, driving the DW toward the right hand disk [i.e., expanding the left hand domain; Fig. 1(b)].

We will concentrate first on pinning induced by a vortex which has a negative core polarity, $p = -1$. Directly beneath the $p = -1$ core, there is a significant negative out-of-plane field, H^z_{vortex} [Fig. 2(a)]. This field "peak" has a width (full width half maximum) on the order of 20 nm and results in there being a localized region in the strip where there is a negative H^z_{vortex} which is strong and opposes the positive H that is used to drive the DW displacement. This localized field acts as a barrier to DW motion, as can be seen in Fig. 2(b) which shows a snapshot of a DW being pinned just to the left of the core center ($w = 48$ nm).

In Fig. 2(c), we follow the normalized z–component of the magnetization within a 36 nm wide strip ($d = 21$ nm) as H is increased by steps, ΔH, enabling us to pass from the pinned state to the depinned state. At very low external fields ($\mu_0 H < 1$ mT), the DW moves towards the disk where it is pinned near the vortex core [as in Fig. 2(b)]. At the depinning field, H_{dep}, the wall depins, moves past the vortex, and annihilates at the end of the strip. Note that while the wall is pinned at the core, the x–component of the magnetization within the vortex increases [also shown in Fig. 2(c)]. This increase corresponds to a shift of the core in the $+y$ direction [Fig. 2(b)] and is driven by the in-plane component of the stray magnetic field ($+x$–oriented) which exists above the domain wall[34–37] [Fig. 2(d)]. This field acts on the vortex's curling magnetization [Fig. 2(e)], inducing a core shift. The direction of this shift depends on the vortex chirality [Figs. 2(f) and 2(g)] since the chirality determines the at-equilibrium core displacement for a given in-plane magnetic field.[38]

We now look at the dependence of the depinning field on the system geometry for the same $p = -1$ vortex configuration. In Figs. 3(a) and 3(b), we show that increasing the strip width, w, or the disk-strip separation, d, will reduce H_{dep}. The latter d-dependence occurs because as d is

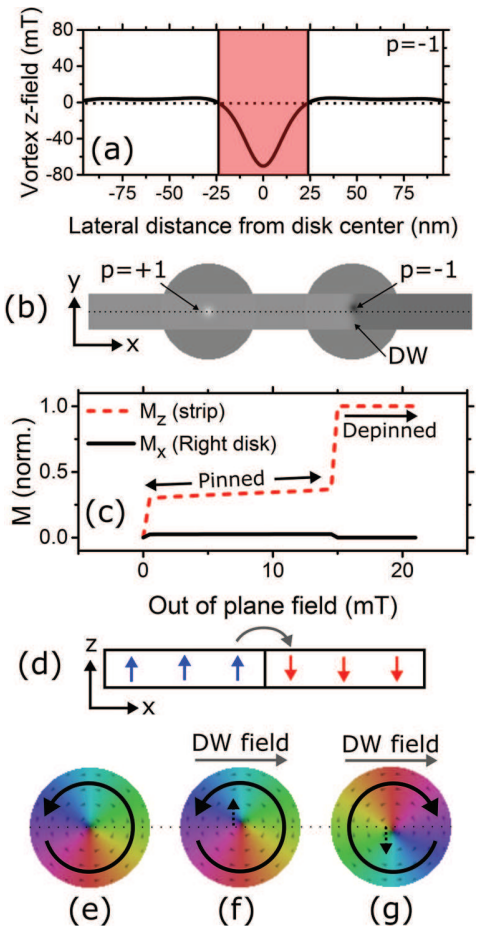

FIG. 2. (a) $z-$component of the stray field generated by a $p = -1$ vortex, H^z_{vortex}, calculated 10.5 nm below the vortex-containing disc. The (red) shaded region shows where $H^z_{\mathrm{vortex}} < 0$ and thus opposes H, generating DW pinning. (b) Bottom-up visualization of a pinned DW ($w = 72$ nm) with gray level mapping of the out-of-plane magnetization component. The DW is at the right hand disk, pinned at the down-magnetized ($p = -1$) vortex core (its position is visible as a dark gray dot). (c) M_z in a $w = 36$ nm strip ($d = 21$ nm) and M_x in the right hand disk (i.e., in the disk at which the DW becomes pinned) as H is increased in steps. (d) An in-plane stray field (arrow) is generated above the DW. (e) Vortex state with a centered core (i.e., negligible in-plane field). The circular arrow indicates the chirality. When the DW is pinned at the vortex, the DW's in-plane stray field (gray arrow) shifts the core in the (f) $+y$ direction for an anti-clockwise vortex or (g) the $-y$ direction for a clockwise vortex. The black dotted line across (e)–(g) marks the position of the unshifted core, and the small dotted arrows in (f) and (g) show the core shift direction.

increased, the strip will be further from the disk and thus subject to a weaker H^z_{vortex}. Since the pinning is H^z_{vortex}-mediated, this leads to a smaller H_{dep}. The w-dependence can be understood as follows: For very narrow strips, the entire strip width is subject to a strong, negative H^z_{vortex} [as can be inferred from Fig. 2(a)], which generates a high H_{dep}. In contrast, for a wide strip, only the central portion of the strip will be subject to the strong H^z_{vortex} which exists directly below the core. As such, the average H^z_{vortex} acting across the strip is lower, leading to a reduced H_{dep}. Indeed, H_{dep} can be shown to closely match the width-averaged H^z_{vortex} both when varying d [Fig. 3(c); $w = 36$ nm] and w [Fig. 3(d); $d = 9$ nm]. Note that H^z_{vortex} was calculated in each case for an isolated vortex subject to $H_{\mathrm{dep}} - \Delta H$ (i.e., at the field preceding that which generated depinning). We also note that the above results were checked with OOMMF[33] for d = 9

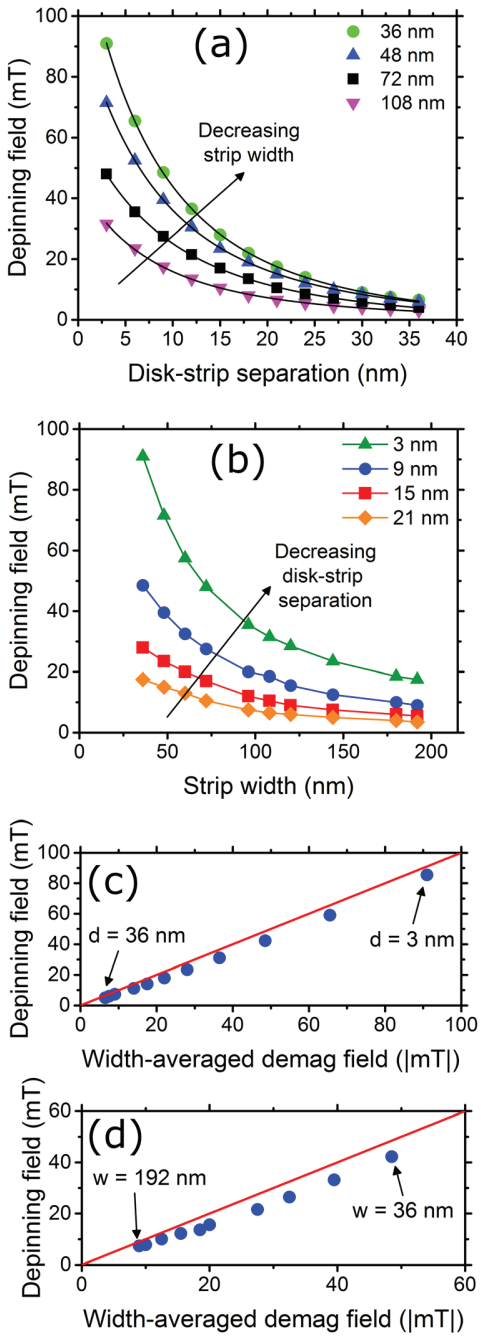

FIG. 3. $p=-1$ depinning field versus (a) disk-strip separation, d, and (b) strip-width, w, for various values of w and d. Black lines in (a) are fits of the form $a+\frac{b}{(c+d)^3}$. Lines in (b) are guides to the eye. Depinning fields for various values of (c) d ($w=36$ nm) and (d) w ($d=9$ nm) plotted against the absolute value of the w-averaged $z-$ component of an isolated vortex's stray magnetic field in the region of the DW. The latter was calculated for an isolated disk in the presence of an out of plane field with magnitude $H=H_{dep}-\Delta H$ (i.e., the field preceding depinning for that particular geometry).

and 15 nm which yielded agreement with the MuMax3-calculated H_{dep} values to within 1 mT. Smaller discretization lengths were also examined using MuMax3 as a further check where reducing the in-plane discretization from 3 nm to 2 nm was found to result in a weak change in the depinning fields (+2.9%).

Switching the polarity of the core to $p=+1$ (achieved by changing the polarity of the pre-relaxation trial vortex state) switches the sign of the vortex stray field, resulting in H^z_{vortex} now being negative (and thus opposing DW motion) in the regions *surrounding* the core position (rather than the region directly beneath the core) [Fig. 4(a); compare to Fig. 2(a) which shows the stray field for $p=-1$]. As a result, the DW now becomes pinned well before it reaches the core [Fig. 4(b)] rather than being pinned at the core location [Fig. 2(b)]. The part of the H^z_{vortex} profile causing pinning for $p=+1$ [Fig. 4(a)] is also much weaker than the part of the profile directly beneath the vortex core, which generates pinning for the $p=-1$ case. This results in H_{dep} being reduced for $p=+1$. This can be seen in Fig. 4(c) where H_{dep} has been plotted versus d for both core polarities ($w=36$ nm). Switching the core polarity (which can be achieved rapidly for quick gate modification[25,26,28,29]) reduces the depinning field by ≈80% over a wide range of d [Fig. 4(d)]. As can be seen in Fig. 4(e), however, H_{dep} for $p=+1$ is almost independent of w (tested for $d=9$ nm). This is consistent with the weak lateral spatial gradient in H^z_{vortex} in the region away from the core [i.e., the part of the vortex-generated field distribution which generates pinning is relatively uniform in space; Fig. 4(a)]. As a result, the %-reduction in H_{dep} when

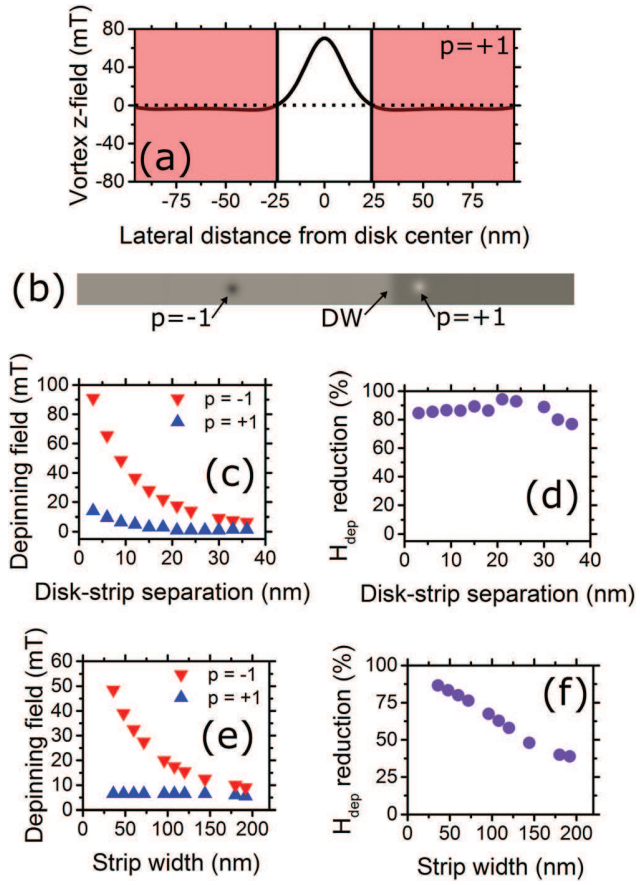

FIG. 4. (a) $z-$component of the stray field generated by a $p=+1$ vortex, H^z_{vortex}, calculated 10.5 nm below the vortex-containing disc. The (red) shaded region shows where $H^z_{vortex}<0$ and thus opposes H, generating DW pinning. (b) Visualization of a pinned DW with gray level mapping of the out-of-plane magnetization component and superposition of the core magnetizations (gray and white dots). The DW is at the right hand disk, pinned well to the left of the right hand vortex core. Lower panels show comparisons of depinning fields for polarities opposing ($p=-1$) and aligned with ($p=+1$) the external field versus (c) d ($w=36$ nm) and (e) w ($d=9$ nm). Corresponding percentage reductions in the depinning fields by switching from $p=+1$ to $p=-1$ are shown in (d) and (f).

going from $p=-1$ to $p=+1$ is largest for small w [Fig. 1(f)] since H_{dep} for $p=-1$ becomes weak at high w due to the averaging effect discussed above [Fig. 3(d)].

We now examine the effect that shifting the core has on domain wall depinning ($p=-1$). To induce a core shift, we apply an in-plane magnetic field which is constant in time, H_{IP}. H_{IP} is aligned along the strip's long axis ($+x$), acting to shift the core perpendicular to that axis ($+y$). H_{dep} versus H_{IP} is plotted for four strip widths in Fig. 5 together with a visualization of the out-of-plane component of the disk's stray field ($\mu_0 H_{IP} = 21$ mT).

In terms of the H_{IP}-dependence of H_{dep}, two clear regimes are seen for the three narrowest strips. For low H_{IP} (below 12 mT in Fig. 5), H_{dep} initially decreases with the in-plane field. In this regime, shifting the core away from the narrow strips' centers reduces the average H^z_{vortex} that acts on the strip, thereby reducing H_{dep}. The initial drop-off in H_{dep} is the steepest for the narrower strips since the core-displacement-driven change in the strip-width-averaged H^z_{vortex} for small core displacements will be the highest. At higher H_{IP}, H_{dep} begins to increase with H_{IP}. In this regime, the core becomes pinned at the vortex core and then again at the disk's right edge. This second pinning event arises due to the $+x$ in-plane field transitioning the disk toward a $+x$-magnetized state. This induces edge magnetic charges on the $\pm x$ sides of the disk which generate out-of-plane stray fields that act on the strip (inset of Fig. 5). The out-of-plane components of the edge fields are negative on the disk's right hand side and can thus pin the domain wall. Furthermore, the strength of these edge fields grows with H_{IP} as the disk acquires a higher $+x$ magnetization. The edge pinning mechanism dominates core-induced pinning at large H_{IP}, leading to an increasing H_{dep}. Note that compared to the core stray field, these edge fields are relatively uniform in the y-direction (Fig. 5), which results in similar H_{dep} values for each strip width. Finally, we note that H_{dep} in the 192 nm strip exhibits a monotonically increasing trend with the in-plane field, which is similar to that seen for the narrow strips at high fields where depinning requires the wall to move past the edge-charge-generated pinning. Indeed, from 6 mT onwards, in the $w=192$ nm strip, pinning due to edge charges dominates the core-mediated pinning, the latter being intrinsically weak at large w [Fig. 3(b)].

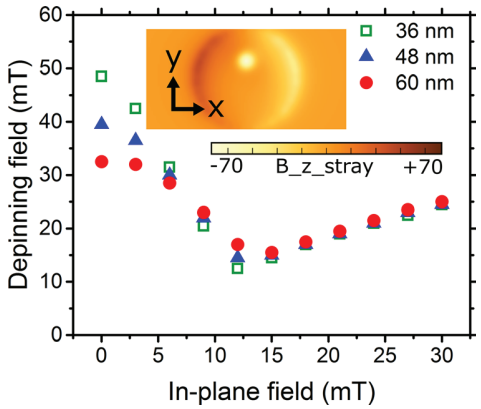

FIG. 5. Depinning field versus in-plane field for four strip widths at $d=9$ nm. The field is applied in the $+x$ direction, shifting the core in the $+y$ direction. The inset shows the z-component of the stray field below a shifted vortex core ($p=-1$) in an isolated disk, as calculated at the vertical center of the strip region for $d=9$ nm in a $+x$-oriented in-plane magnetic field of $+21$ mT (color scale bar for the out-of-plane field is also shown in mT). The position of the $+y$ shifted core can be identified by its localized negative field. Stray fields are also generated below the disk's $\pm x$ edges.

In summary, this work demonstrates the potential to use localized stray magnetic fields generated by vortex states to reliably generate reconfigurable, nano-scale domain wall pinning sites in an underlying perpendicularly magnetized ferromagnetic strip. The domain wall pinning strength can be tuned by switching the vortex core polarity or by shifting the core across the strip (done here via in-plane magnetic fields). This approach enables the development of controllable gates for domain wall motion and logic. These findings also open possibilities for further investigations on harnessing magnetostatic interactions between skyrmions[39] and domain walls (or skyrmions and vortices). Extensions to current-induced manipulation of magnetic textures may also be envisaged. There will also be interesting effects to examine full dynamic simulations where one can aim to (e.g.) rapidly toggle the pinning strength (via a switch in the core magnetization or a well-timed core displacement) or dynamically study core displacements (or core-polarity-switching[40]) driven by domain-wall-vortex interactions.

This work was supported by resources provided by the Pawsey Supercomputing Centre with funding from the Australian Government and the Government of Western Australia. The preliminary work was supported by iVEC through the use of advanced computing resources located at iVEC@UWA. P.J.M. acknowledges support from the Australian Research Council's Discovery Early Career Researcher Award scheme (Grant No. DE120100155) and the University of Western Australia (Research Development Award and Early Career Researcher Fellowship Support schemes). A.C.H.H. and J.A.I. were supported by internships from the Pawsey Supercomputing Centre and iVEC, respectively. The authors thank H. Fangohr, M. Albert, R. L. Novak, M. Kostylev, and J. P. Fried for useful discussions.

[1]D. A. Allwood, G. Xiong, C. C. Faulkner, D. Atkinson, D. Petit, and R. P. Cowburn, Science **309**, 1688 (2005).
[2]S. Fukami, T. Suzuki, K. Nagahara, N. Ohshima, Y. Ozaki, S. Saito, R. Nebashi, N. Sakimura, H. Honjo, K. Mori, C. Igarashi, S. Miura, N. Ishiwata, and T. Sugibayashi, in 2009 Symposium on VLSI Technology (2009), p. 230.
[3]J. Jaworowicz, N. Vernier, J. Ferré, A. Maziewski, D. Stanescu, D. Ravelosona, A. S. Jacqueline, C. Chappert, B. Rodmacq, and B. Diény, Nanotechnology **20**, 215401 (2009).
[4]S. Breitkreutz, I. Eichwald, J. Kiermaier, G. Hiblot, G. Csaba, W. Porod, D. Schmitt-Landsiedel, and M. Becherer, J. Appl. Phys. **115**, 17D506 (2014).
[5]S. Lequeux, J. Sampaio, V. Cros, K. Yakushiji, A. Fukushima, R. Matsumoto, H. Kubota, S. Yuasa, and J. Grollier, Sci. Rep. **6**, 31510 (2016).
[6]J. A. Currivan-Incorvia, S. Siddiqui, S. Dutta, E. R. Evarts, J. Zhang, D. Bono, C. A. Ross, and M. A. Baldo, Nat. Commun. **7**, 10275 (2016).
[7]O. Boulle, G. Malinowski, and M. Kläui, Mater. Sci. Eng., R **72**, 159 (2011).
[8]J. H. Franken, H. J. M. Swagten, and B. Koopmans, Nat. Nanotechnol. **7**, 499 (2012).
[9]S. S. P. Parkin, M. Hayashi, and L. Thomas, Science **320**, 190 (2008).

[10]G. Rowlands, see https://github.com/grahamrow/muview2 for "Muview2 micromagnetic viewer".
[11]J. H. Franken, Y. Yin, A. J. Schellekens, A. van den Brink, H. J. M. Swagten, and B. Koopmans, Appl. Phys. Lett. **103**, 102411 (2013).
[12]A. Bernand-Mantel, L. Herrera-Diez, L. Ranno, S. Pizzini, J. Vogel, D. Givord, S. Auffret, O. Boulle, I. M. Miron, and G. Gaudin, Appl. Phys. Lett. **102**, 122406 (2013).
[13]P. J. Metaxas, P. J. Zermatten, J. P. Jamet, J. Ferré, G. Gaudin, B. Rodmacq, A. Schuhl, and R. L. Stamps, Appl. Phys. Lett. **94**, 132504 (2009).
[14]L. O'Brien, D. Petit, E. R. Lewis, R. P. Cowburn, D. E. Read, J. Sampaio, H. T. Zeng, and A. V. Jausovec, Phys. Rev. Lett. **106**, 087204 (2011).
[15]R. Hiramatsu, T. Koyama, H. Hata, T. Ono, D. Chiba, S. Fukami, and N. Ishiwata, J. Korean Phys. Soc. **63**, 608 (2013).
[16]P. J. Metaxas, P. J. Zermatten, R. L. Novak, S. Rohart, J. P. Jamet, R. Weil, J. Ferré, A. Mougin, R. L. Stamps, G. Gaudin, V. Baltz, and B. Rodmacq, J. Appl. Phys. **113**, 073906 (2013).
[17]J. H. Franken, M. A. J. van der Heijden, T. H. Ellis, R. Lavrijsen, C. Daniels, D. McGrouther, H. J. M. Swagten, and B. Koopmans, Adv. Funct. Mater. **24**, 3508 (2014).
[18]R. A. van Mourik, C. T. Rettner, B. Koopmans, and S. S. P. Parkin, J. Appl. Phys. **115**, 17D503 (2014).
[19]R. P. Cowburn, D. K. Koltsov, A. O. Adeyeye, and M. E. Welland, Phys. Rev. Lett. **83**, 1042 (1999).
[20]T. Shinjo, T. Okuno, R. Hassdorf, K. Shigeto, and T. Ono, Science **289**, 930 (2000).
[21]A. Wachowiak, J. Wiebe, M. Bode, O. Pietzsch, M. Morgenstern, and R. Wiesendanger, Science **298**, 577 (2002).
[22]R. L. Novak and L. C. Sampaio, e-print arXiv:1702.02451.
[23]L. O'Brien, D. Petit, H. T. Zeng, E. R. Lewis, J. Sampaio, A. V. Jausovec, D. E. Read, and R. P. Cowburn, Phys. Rev. Lett. **103**, 077206 (2009).
[24]L. Rondin, J. P. Tetienne, S. Rohart, A. Thiaville, T. Hingant, P. Spinicelli, J. F. Roch, and V. Jacques, Nat. Commun. **4**, 2279 (2013).
[25]K. Yamada, S. Kasai, Y. Nakatani, K. Kobayashi, and T. Ono, Appl. Phys. Lett. **93**, 152502 (2008).
[26]M. Noske, A. Gangwar, H. Stoll, M. Kammerer, M. Sproll, G. Dieterle, M. Weigand, M. Fähnle, G. Woltersdorf, C. H. Back, and G. Schütz, Phys. Rev. B **90**, 104415 (2014).
[27]T. Okuno, K. Shigeto, T. Ono, K. Mibu, and T. Shinjo, J. Magn. Magn. Mater **240**, 1 (2002).
[28]B. Van Waeyenberge, A. Puzic, H. Stoll, K. W. Chou, T. Tyliszczak, R. Hertel, M. Fähnle, H. Brückl, K. Rott, G. Reiss, I. Neudecker, D. Weiss, C. H. Back, and G. Schütz, Nature **444**, 461 (2006).
[29]K. Yamada, S. Kasai, Y. Nakatani, K. Kobayashi, H. Kohno, A. Thiaville, and T. Ono, Nat. Mater. **6**, 270 (2007).
[30]N. Usov and S. Peschany, J. Magn. Magn. Mater. **118**, L290 (1993).
[31]E. Martinez, L. Torres, and L. Lopez-Diaz, Phys. Rev. B **83**, 174444 (2011).
[32]A. Vansteenkiste, J. Leliaert, M. Dvornik, M. Helsen, F. Garcia-Sanchez, and B. Van Waeyenberg, AIP Adv. **4**, 107133 (2014).
[33]M. J. Donahue and D. G. Porter, "OOMMF user's guide, version 1.0, interagency report NISTIR 6376," Technical Report NISTIR 6376 (National Institute of Standards and Technology, Gaithersburg, MD, 1999).
[34]S. Wiebel, J. P. Jamet, N. Vernier, A. Mougin, J. Ferré, V. Baltz, B. Rodmacq, and B. Dieny, Appl. Phys. Lett. **86**, 142502 (2005).
[35]S. Wiebel, J. P. Jamet, N. Vernier, A. Mougin, J. Ferré, V. Baltz, B. Rodmacq, and B. Dieny, J. Appl. Phys. **100**, 043912 (2006).
[36]A. Bellec, S. Rohart, M. Labrune, J. Miltat, and A. Thiaville, Europhys. Lett. **91**, 17009 (2010).
[37]P. J. Metaxas, R. L. Stamps, J. P. Jamet, J. Ferré, V. Baltz, and B. Rodmacq, J. Phys.: Condens. Matter **24**, 024212 (2012).
[38]M. Schneider, H. Hoffmann, and J. Zweck, Appl. Phys. Lett. **79**, 3113 (2001).
[39]J. Sampaio, V. Cros, S. Rohart, A. Thiaville, and A. Fert, Nature Nanotechnol. **8**, 839 (2013).
[40]P. Wohlhüter, M. T. Bryan, P. Warnicke, S. Gliga, S. E. Stevenson, G. Heldt, L. Saharan, A. K. Suszka, C. Moutafis, R. V. Chopdekar, J. Raabe, T. Thomson, G. Hrkac, and L. J. Heyderman, Nat. Commun. **6**, 7836 (2015).